HYDROLOGICAL PROCESSES
Hydrol. Process. (2008)
Published online in Wiley InterScience
(www.interscience.wiley.com) DOI: 10.1002/hyp.6930

Modelling longwave radiation to snow beneath forest canopies using hemispherical photography or linear regression

Richard Essery,[1]* John Pomeroy,[2] Chad Ellis[2] and Tim Link[3]

[1] *School of Geosciences, University of Edinburgh, Edinburgh EH9 3JW, UK*
[2] *Centre for Hydrology, University of Saskatchewan, Saskatoon, Canada*
[3] *University of Idaho, Moscow, ID, USA*

Abstract:

Forest canopies reduce shortwave radiation and increase longwave radiation reaching the underlying surface, compared with open areas, and thus influence rates at which forest snowpacks melt. The sub-canopy radiative environment can be highly heterogeneous, with temporal persistence depending on canopy structure and differing for shortwave and longwave fluxes, and this influences the rate at which snow-free ground emerges during snowmelt. Arrays of radiometers have been used to measure spatial variability in forest radiation, but such instruments are expensive and require regular attention in snowy environments. Hemispherical photography allows rapid collection of canopy structure data, and many software packages have been developed for modelling transmission of shortwave radiation using hemispherical photographs, but modelling of longwave radiation has received much less attention. Results are used here from radiometers located beneath lodgepole pine stands of varying density at the Marmot Creek Research Basin in Alberta, Canada. A simple model using sky view calculated from hemispherical photographs to weight longwave emissions from the canopy, calculated using measured air temperature as a proxy for canopy temperature, and measured above-canopy longwave radiation is found to give good estimates for spatial averages of sub-canopy longwave radiation, although standard deviations are generally underestimated. If above-canopy longwave radiation is parametrized as a function of air temperature and humidity rather than measured, good results are still obtained for daily and longer averages of sub-canopy longwave radiation. A multiple linear regression model using measurements of above-canopy shortwave radiation to estimate daytime canopy heating gives better results in comparison with individual radiometers. Copyright © 2008 John Wiley & Sons, Ltd.

KEY WORDS forest snow; canopy radiation modelling; longwave radiation; hemispherical photography

Received 1 July 2007; Accepted 10 October 2007

INTRODUCTION

Snow under forests is the source of the greatest proportion of streamflow in Canadian mountain and boreal forest regions (Gray, 1970) and is known to be very sensitive to canopy structure (Metcalfe and Buttle, 1998; Sicart *et al*., 2004). Canopy structure varies widely across boreal and mountain forests from relatively open deciduous and taiga stands to dense spruce and fir stands. This structure can also change rapidly due to fire, harvesting, clearing for agriculture and insect infestations such as mountain pine beetle. It is expected to change further due to rapid recent and anticipated climate warming (Danby and Hik, 2007). Forest canopies strongly influence radiative fluxes reaching the sub-canopy surface, and so influence temperatures and melt rates for forest snowpacks. Shortwave radiation is reduced by forest shading, but longwave radiation is increased during the day as canopy elements are heated by absorption of solar radiation, and during the night as the canopy generally has a higher thermal emissivity than the unobstructed sky. Sub-canopy radiation is also highly heterogeneous, with higher shortwave radiation in sunflecks and higher longwave radiation close to sunlit trunks; spatial variance in radiation influences the average rate of snowmelt if there is a covariance with the spatial distribution of sub-canopy snow (Faria *et al*., 2000). Forest hydrology snowmelt models often estimate the longwave contribution as part of a sub-canopy net radiation that is a linear function of above-canopy net radiation, often by calibration of coefficients to the hydrograph. The assumption behind these methods is that net radiation above and below the canopy are well correlated, and the strength of this assumption is now well known. Avoiding such an assumption requires explicit calculation of short- and longwave radiation under forest canopies. This is desirable not only for accurate mean melt energy calculations, but also in order to investigate the spatial distribution of melt energy under the canopy and the effects that this may have on snow cover depletion, and hence, areal melt rates.

Some sophisticated land surface models (e.g. Sellers *et al*., 1986; Verseghy *et al*., 1993) predict radiative fluxes beneath vegetation canopies, but these models have high data requirements for meteorological inputs and model parameters. Simple techniques using limited data are needed for practical applications. Hemispherical photography provides a rapid method for gathering canopy

* Correspondence to: Richard Essery, School of Geosciences, University of Edinburgh, Edinburgh EH9 3JW, UK. E-mail: richard.essery@ed.ac.uk

structure data in the field; the use of hemispherical photography for studying forest light environments has a long history (e.g. Evans and Coombe, 1959; Anderson, 1964), and many software packages such as GLA (Frazer *et al*., 1999) and Hemiview (Rich *et al*., 1999) have been developed for processing hemispherical images. Hemispherical photography has also been used in studies of sub-canopy snow distributions (Lundberg *et al*., 2004; López-Moreno and Latron, 2008). Prediction of shortwave radiation is relatively straightforward, being largely determined by canopy geometry and above-canopy radiation, but prediction of longwave radiation requires additional information on canopy temperatures (Pomeroy *et al*., 2007) and has received much less attention. Accurate measurements of canopy temperature are rarely available, except at well-instrumented research sites, but air temperature is more commonly measured; it may be that air temperature can be used as a proxy for canopy temperature in sufficiently dense forests with limited direct solar heating of the parts of the canopy visible from the ground (Sicart *et al*., 2004).

In this paper, we test the accuracy with which longwave radiation can be predicted beneath coniferous canopies of varying density using hemispherical photography and measurements of air temperature but no information on canopy temperatures, either with or without measured above-canopy longwave radiation. Multiple linear regression is used to assess by how much these predictions can be improved if above-canopy shortwave radiation measurements are also available, and relationships between the regression coefficients and hemispherical sky view are investigated. The accuracy with which regression coefficients obtained from short periods of sub-canopy radiation measurements can be used to make long-term radiation predictions is tested.

SITE DESCRIPTIONS

The study was conducted in and near the Marmot Creek Research Basin, Alberta, Canada (50°57′N, 115°09′W). Elevations in the basin range from 1350 to 3100 metres above sea level (m.a.s.l.), of which the lower parts are covered by lodgepole pine forest (*Pinus contorta* var. *Latifolia*). Fluxes of incoming longwave radiation were measured beneath two lodgepole pine canopies and in one small clearing, all of which had melting snow on the ground. Sites were established at a southeast-facing slope (125° azimuth, 26° slope) with discontinuous canopy cover and non-uniform tree sizes at 1563 m.a.s.l., a level forest with continuous canopy cover and uniform tree sizes at 1528 m.a.s.l., and a small level forest gap in a camp ground south of Marmot Creek; photographs of the sites are shown in Figure 1. Reference incoming shortwave and longwave fluxes were measured in a large level clearing and taken to be representative of above-canopy radiation. Sub-canopy radiation was measured using an array of ten Kipp and Zonen CM3 shortwave pyranometers and ten Eppley PIR longwave pyrgeometers controlled by Campbell Scientific CR10X dataloggers programmed to store 5-min averages of measurements made every 10 s. Fairall *et al*. (1998) estimated the precision of the PIR measurements to be 1·5% (∼5 Wm^{-2}), and the radiometers are regularly tested in side-by-side comparisons. Link *et al*. (2004) and Essery *et al*. (2007) discuss confidence levels for statistics calculated from array measurements in forests. Although the radiometer array was only run for a short period at each site, longer data records are available from several fixed longwave radiometers: one at the level forest site, three at the southeast-facing forest site and one at a nearby north-facing forest site. Fifteen-minute averages are recorded for these radiometers.

Spatial variations in sub-canopy radiation were measured by placing the longwave and shortwave radiometers on the ground in pairs at each site. The radiometer pairs were distributed randomly within circles of 7 m radius (determined by the cable length) around central logger positions in the level and southeast-facing forest sites, but they were placed along a 14-m line running across the forest gap site from the south to a few metres back under the canopy on the north of the gap. The radiometers were inclined to the local slope at the southeast-facing forest site but were levelled at the other sites, so sub-canopy radiation in this paper *always* refers to fluxes perpendicular to the surface. Three days of data were obtained at each site, the array being run for 11–13 March 2005 in the southeast-facing forest, 15–17 March 2005 in the level forest and 14–16 March 2006 in the forest gap. Sub-canopy measurements of air temperature and humidity were available for the level and southeast-facing forest sites but not for the forest gap; data from

Figure 1. Photographs of (a) the southeast-facing forest site, (b) the level forest site and (c) the forest gap site (showing several of the radiometer pairs)

DOI: 10.1002/hyp

the level forest will be used for this site when required. Above-canopy shortwave and longwave radiation for the periods of the sub-canopy measurements are shown in Figure 2; a range of weather conditions was experienced, but there were no completely clear or completely overcast days.

The forest canopies were characterized by taking hemispherical photographs above each radiometer. The camera was levelled for photographs taken at the level forest and forest gap sites but set parallel to the slope at the southeast-facing forest site. A manually selected brightness threshold was applied to each photograph to make canopy masks; examples are shown in Figure 3 for one radiometer location in each of the level and southeast-facing forests and for the radiometer locations with greatest and least canopy closure in the forest gap site. Because the camera was tilted to match the slope, the trunks appear curved in Figure 3(a) and some ground is included in the hemispherical view.

LONGWAVE RADIATION MODELLING

Downward longwave radiation at a point beneath a forest canopy is given by

$$L\downarrow = vL_{\downarrow 0} + (1 - v)\sigma T_c^4 \tag{1}$$

where v is the sky view factor for the sub-canopy point, $L_{\downarrow 0}$ is the above-canopy longwave radiation, σ is the Stefan-Boltzmann constant and T_c is the canopy temperature; because different parts of the canopy will have different temperatures and the canopy emissivity will not be exactly equal to 1, this is an effective radiative temperature for the visible parts of the canopy. The sky view is calculated as

$$v = \frac{1}{\pi}\int_0^{\pi/2} d\theta \int_0^{2\pi} d\varphi \sin\theta\cos\theta\ c(\theta, \varphi) \tag{2}$$

where c is 0 if the sky is obscured by canopy or ground at elevation angle θ and azimuth φ and is 1 otherwise. For

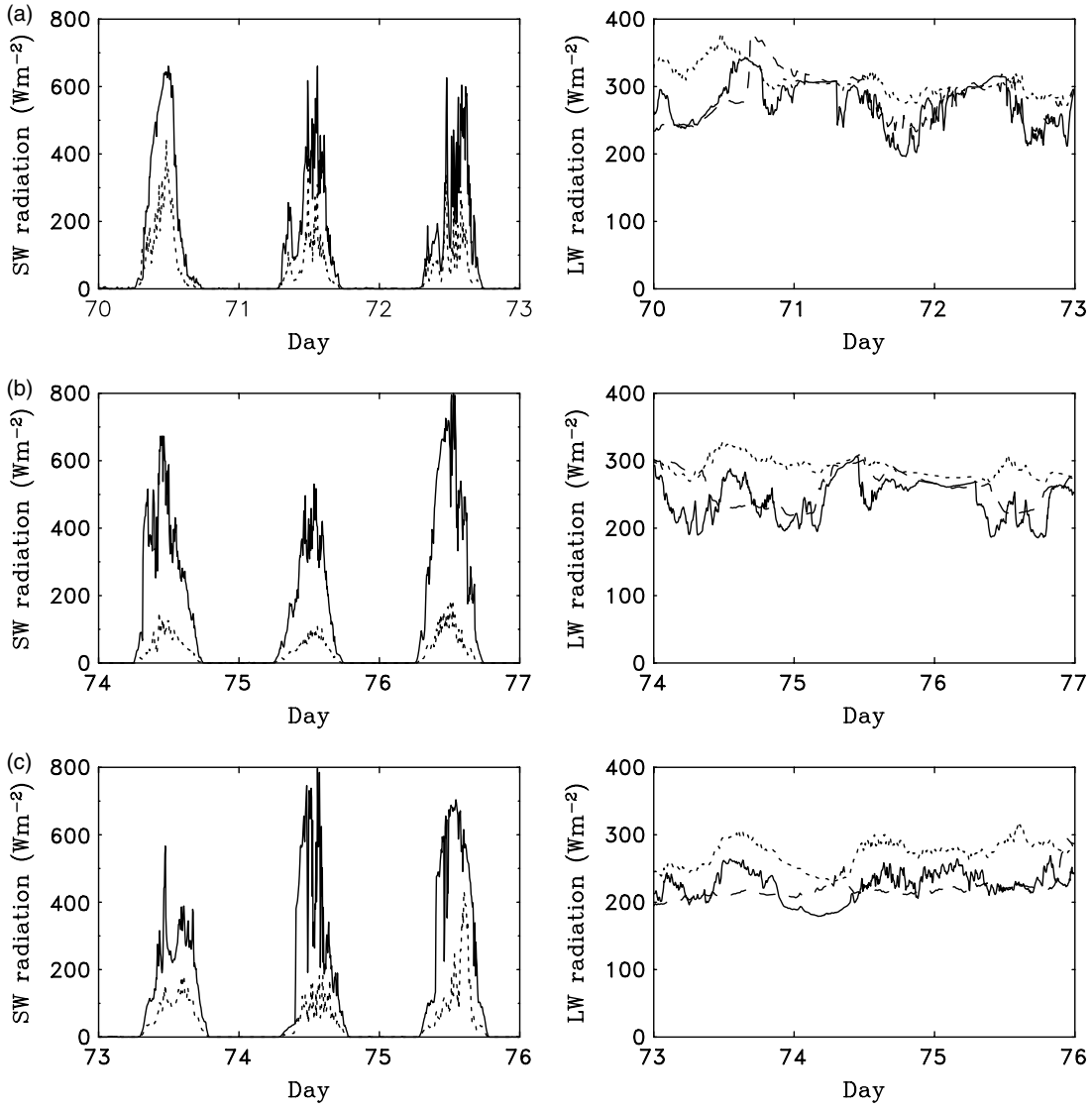

Figure 2. Shortwave radiation (left) and longwave radiation (right) measured above (solid lines) and below (dotted lines) the canopies for the periods that sub-canopy radiometer arrays were deployed in (a) the southeast-facing forest, (b) the level forest and (c) the forest gap. Dashed lines show modelled above-canopy longwave radiation

DOI: 10.1002/hyp

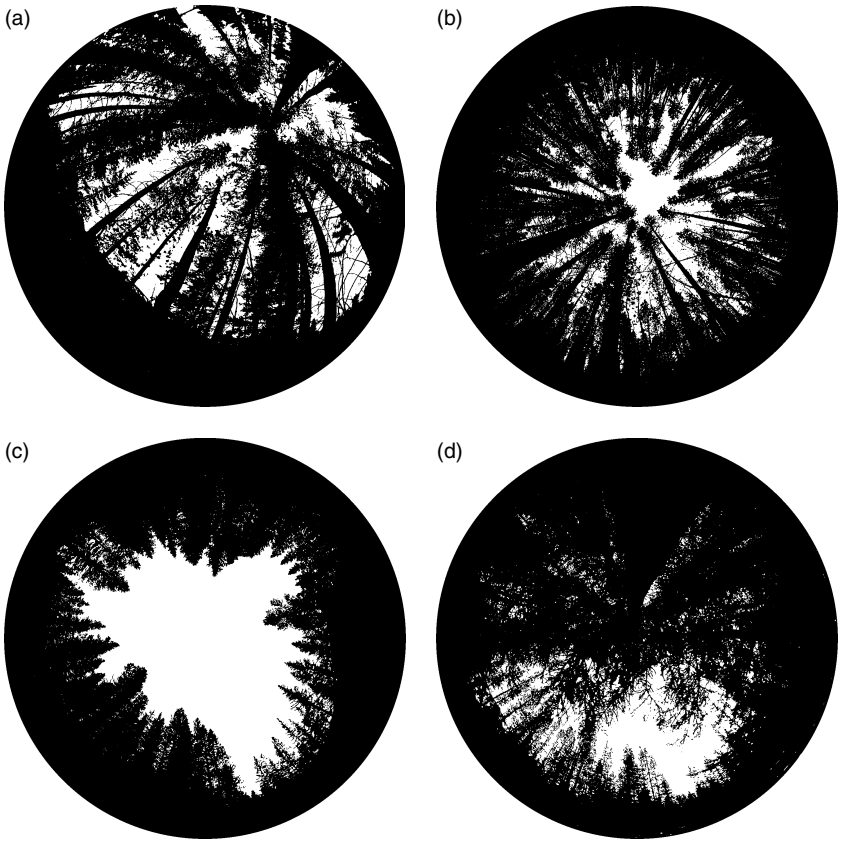

Figure 3. Examples of hemispherical images for (a) radiometer 10 in the southeast-facing forest, (b) radiometer 5 in the level forest, (c) radiometer 3 in the forest gap and (d) radiometer 7 under a tree at the north end of the forest gap. Skyview factors for these images are 0·26, 0·25, 0·52 and 0·20 respectively

an equiangular hemispherical lens projection, direction (θ,φ) maps onto a point (x,y) on the image, measured from the centre, such that

$$\theta = \frac{\pi}{2}\left[1 - \frac{(x^2+y^2)^{1/2}}{r}\right] \tag{3}$$

and

$$\varphi = \tan^{-1}\left(\frac{y}{x}\right) \tag{4}$$

where r is the radius of the horizon circle on the image. Sky view can be calculated from digital hemispherical images by dividing the image into n_θ elevation bands and n_φ azimuth bands, and discretizing Equation (2) as

$$v = \frac{\pi}{n_\theta n_\varphi}\sum_{i=1}^{n_\theta}\sum_{j=1}^{n_\varphi}\sin\theta_i\cos\theta_i\ c(\theta_i,\varphi_j). \tag{5}$$

Sky views for each of the radiometer locations are given in Tables I–IV.

Table I. Statistics for the southeast-facing forest site. The columns, from left to right, are radiometer number, sky view, average enhancement of longwave radiation by the canopy, bias and root mean square (rms) errors and r^2 obtained using measured above-canopy longwave radiation ($L_{\downarrow 0}$), bias and rms errors and r^2 obtained using modelled above-canopy longwave radiation ($L_{\downarrow \mathrm{m}}$), and rms errors and r^2 for multiple linear regression (mlr)

Radiometer	v	$L_\downarrow - L_{\downarrow 0}$	$L_{\downarrow 0}$			$L_{\downarrow \mathrm{m}}$			mlr	
			bias	rms	r^2	bias	rms	r^2	rms	r^2
1	0·49	25·29	−1·04	8·03	0·88	2·45	17·19	0·48	6·35	0·92
2	0·48	23·47	1·15	7·31	0·90	4·58	16·92	0·50	6·11	0·93
3	0·18	41·39	−2·86	8·80	0·89	−1·53	10·41	0·84	5·78	0·95
4	0·39	27·01	1·92	7·16	0·90	4·70	14·69	0·60	6·08	0·92
5	0·32	33·03	−0·87	7·08	0·90	1·42	12·33	0·69	5·16	0·94
6	0·29	35·04	−1·34	8·19	0·87	0·71	12·10	0·72	5·68	0·94
7	0·31	35·33	−2·72	7·79	0·89	−0·50	11·98	0·70	5·50	0·94
8	0·27	38·86	−4·14	8·98	0·88	−2·24	11·64	0·75	5·82	0·94
9	0·24	40·02	−4·24	9·24	0·88	−2·50	11·48	0·78	5·78	0·94
10	0·26	38·76	−3·63	8·87	0·87	−1·79	11·53	0·75	5·84	0·93
Mean	0·32	33·82	−1·78	7·34	0·90	0·53	12·30	0·69	5·22	0·94

DOI: 10.1002/hyp

Table II. As Table I, but for the level forest

Radiometer	v	$L_{\downarrow} - L_{\downarrow 0}$	$L_{\downarrow 0}$			$L_{\downarrow \mathrm{m}}$			mlr	
			bias	rms	r^2	bias	rms	r^2	rms	r^2
1	0·24	48·96	−8·10	9·97	0·84	−4·19	8·95	0·68	2·70	0·96
2	0·25	47·20	−6·98	8·89	0·85	−2·87	8·65	0·64	2·97	0·95
3	0·26	46·40	−6·51	8·67	0·84	−2·30	8·51	0·65	3·09	0·95
4	0·25	48·41	−7·76	9·94	0·81	−3·78	9·16	0·63	3·09	0·95
5	0·25	46·97	−6·50	8·67	0·84	−2·46	8·65	0·63	2·92	0·95
6	0·25	45·91	−5·56	8·17	0·83	−1·49	8·82	0·61	2·95	0·96
7	0·27	46·65	−7·43	9·42	0·84	−3·03	9·29	0·60	2·86	0·96
8	0·28	46·14	−7·29	9·39	0·83	−2·77	9·53	0·59	3·10	0·95
9	0·26	45·71	−5·97	8·27	0·84	−1·72	9·19	0·58	3·13	0·95
10	0·29	45·14	−6·99	9·00	0·84	−2·26	8·79	0·62	3·06	0·95
Mean	0·26	46·75	−6·91	8·93	0·84	−2·69	8·82	0·63	2·73	0·96

Table III. As Table I, but for the forest gap

Radiometer	v	$L_{\downarrow} - L_{\downarrow 0}$	$L_{\downarrow 0}$			$L_{\downarrow \mathrm{m}}$			mlr	
			bias	rms	r^2	bias	rms	r^2	rms	r^2
1	0·37	44·93	2·42	5·81	0·93	0·19	11·08	0·70	4·99	0·93
2	0·50	34·11	3·59	6·32	0·94	0·58	14·57	0·46	4·90	0·94
3	0·52	34·51	1·59	5·46	0·94	−1·54	15·11	0·44	4·67	0·95
4	0·50	33·10	4·56	7·56	0·93	1·56	15·90	0·44	5·09	0·94
5	0·47	37·62	2·22	6·08	0·94	−0·61	14·34	0·53	4·82	0·94
6	0·42	41·97	1·93	6·26	0·93	−0·58	13·23	0·63	4·79	0·95
7	0·20	65·81	−5·28	9·91	0·87	−6·45	11·12	0·90	6·18	0·92
8	0·35	49·51	−0·55	7·40	0·90	−2·65	12·54	0·74	5·89	0·92
9	0·20	65·19	−4·76	9·02	0·89	−5·95	10·42	0·93	5·60	0·93
10	0·24	66·27	−9·21	11·82	0·89	−10·67	13·55	0·93	5·18	0·94
Mean	0·38	47·30	−0·35	5·70	0·93	−2·61	11·72	0·73	4·59	0·95

Table IV. Statistics for sub-canopy longwave radiation predicted by multiple linear regression for the five long-term radiometers. Results are given separately for the calibration period (11–20 March 2005) and the evaluation period (21 March–19 July 2005)

Aspect	v	Calibration			Evaluation				Daily rms
		$L_{\downarrow} - L_{\downarrow 0}$	rms	r^2	$L_{\downarrow} - L_{\downarrow 0}$	bias	rms	r^2	
Southeast	0·28	36·02	3·11	0·98	54·46	−0·63	4·96	0·98	3·26
Southeast	0·49	22·99	8·19	0·85	29·86	−0·77	9·68	0·92	4·96
Southeast	0·31	31·60	3·66	0·97	49·53	−1·01	5·56	0·98	3·59
Level	0·28	32·08	4·77	0·95	44·86	−3·43	6·76	0·98	5·08
North	0·19	37·75	2·56	0·99	53·70	−2·06	3·76	0·99	2·93

Three simple parametrizations of Equation (1) are tested in the next section, each with different data requirements. The first model uses measurements of above-canopy longwave radiation and sub-canopy air temperature with sky view obtained from hemispherical images. The effective canopy temperature is simply assumed to be equal to the air temperature, T_a. Expanding Equation (1) to first order in the difference between canopy and air temperatures, errors in sub-canopy longwave radiation due to this assumption are related to temperature differences by

$$\Delta L_{\downarrow} \approx 4(1 - v)\sigma T_a^3 (T_c - T_a). \quad (6)$$

Errors might be expected to be largest on clear days and close to sunlit trunks due to shortwave heating. Canopy temperatures can fall below air temperatures on clear nights due to longwave radiative cooling, but thermal inertia might keep trunk temperatures above air temperatures overnight. Measurements of canopy temperatures for some of the same sites used here are discussed by Pomeroy *et al.* (2007).

Longwave radiation is absorbed and emitted from the atmosphere depending on temperature and humidity profiles, with much of the incoming radiation at the surface emanating from the lower layers of the atmosphere. When measurements of neither incoming longwave radiation nor atmospheric profiles have been available, many studies of snowmelt modelling (e.g. Yang *et al.*, 1997; Slater *et al.*, 2001; Bowling *et al.*, 2003) have modelled longwave radiation as a function of near-surface air

DOI: 10.1002/hyp

temperature and humidity. A second sub-canopy longwave radiation model is tested here with measurements of $L_{\downarrow 0}$ replaced by modelled values using the method of Iziomon *et al.* (2003), as implemented in the MicroMet model of Liston and Elder (2006). This uses measured air temperature and humidity to calculate an effective atmospheric emissivity, including the influence of modelled cloud cover, to give $L_{\downarrow 0} = \varepsilon_0 \sigma {T_a}^4$. The atmospheric emissivity is modelled by

$$\varepsilon_0 = \kappa(1 + Z f_c^2)\left[1 - X \exp\left(-Y \frac{e}{T_a}\right)\right] \qquad (7)$$

where κ is a calibration parameter (Liston and Elder, 2006), X, Y and Z are height-dependent parameters (Iziomon *et al.*, 2003), e (Pa) is vapour pressure and f_c is the fraction of cloud cover, parametrized as

$$f_c = 0{\cdot}832 \exp\left(\frac{\mathrm{RH}_{700} - 100}{41{\cdot}6}\right) \qquad (8)$$

for relative humidity RH_{700} (%) at 700 mb height, obtained by applying fixed lapse rates to the near-surface air temperature and dew point (Liston and Elder, 2006).

Canopy temperatures are rarely measured, and the appropriate canopy temperature for Equation (1) is some weighted average of temperatures for sunlit and shaded trunks, branches and foliage (Pomeroy *et al.*, 2007). It might be expected, however, that the largest differences between canopy and air temperatures will occur when canopy elements are heated by shortwave radiation on sunny days, and better simulations might be achieved if measurements of above-canopy incoming shortwave radiation $S_{\downarrow 0}$ are available. This possibility is tested by fitting a third model

$$L_\downarrow = c_0 + c_L L_{\downarrow 0} + c_T \sigma T_a^4 + c_s S_{\downarrow 0} \qquad (9)$$

to measurements from each pyrgeometer by multiple linear regression, where c_0 is a constant and c_L, c_T and c_S are weightings for longwave radiation, air temperature and shortwave radiation. If canopy radiative temperatures were exactly equal to air temperatures, the expected coefficients would be $c_0 = 0$, $c_L = v$, $c_T = 1 - v$ and $c_s = 0$. If it is non-zero, c_s can be interpreted as the efficiency with which shortwave radiation is absorbed by the canopy and converted to downwards longwave radiation.

RESULTS

Spatial averages of measured sub-canopy longwave and shortwave radiation are compared with above-canopy radiation in Figure 2. Shortwave radiation is reduced beneath the canopies, particularly for the dense canopy at the level forest site. Although most of the radiometers at the forest gap site were not beneath a canopy, the shortwave radiation is still reduced because the gap is shaded by trees to the south. Above-canopy shortwave radiation is lower on cloudier days, but larger fractions are transmitted to the forest floors. Longwave radiation is increased beneath the canopies, but differences between above-canopy and sub-canopy longwave radiation are lower during cloudy periods because the emissivity of the sky visible through canopy gaps is increased and heating of the canopy by shortwave radiation is reduced.

Array measurements with short averaging periods show high spatial variability in sub-canopy radiation, particularly for the strong bimodal distribution of shortwave radiation in sunflecks and shadows on clear days. For processes such as cumulative snowmelt that integrate the surface energy balance over time, it is important to consider how static the patterns of sub-canopy radiation are (Essery *et al.*, 2007). Figure 4 shows spatial standard deviations calculated from array data with varying time averaging periods from 5 min to 3 days. Standard deviations of shortwave radiation decrease strongly as the averaging period increases, but standard deviations of longwave radiation remain nearly constant; patterns

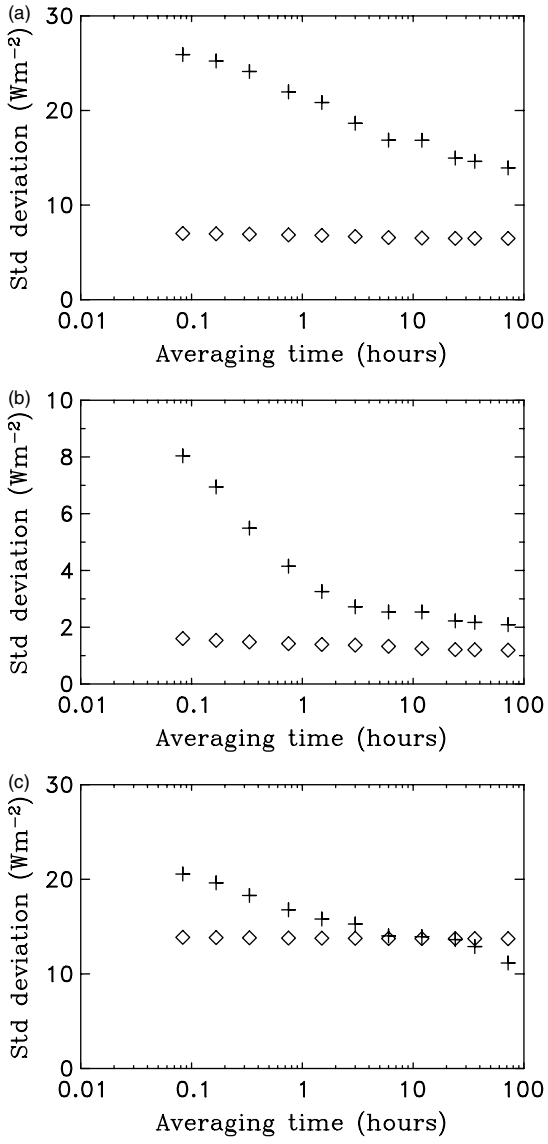

Figure 4. Spatial standard deviations of shortwave (+) and longwave (◊) radiation for varying averaging periods in (a) the southeast-facing forest, (b) the level forest and (c) the forest gap

DOI: 10.1002/hyp

of light and shade move across the surface as the sun moves during the day, and patterns of canopy heating change, but patterns of sub-canopy longwave enhancement due to restricted sky view and increased emissivity under canopies remain fixed. For the forest gap site, the standard deviation of longwave radiation actually exceeds that for shortwave radiation for averaging periods longer than a day.

Time series of averages and standard deviations of sub-canopy longwave radiation calculated from Equation (1) with air temperature as a proxy for canopy temperature are compared with measurements for each site in Figure 5, and statistics for individual radiometers are given in Tables I–III. Averages of measured and modelled longwave radiation are within 9 Wm^{-2} of each other and root mean square (rms) errors are less than 10 Wm^{-2} for all radiometers except for one (radiometer 10) under the canopy at the north of the forest gap site; correlation of measured and modelled time series gives r^2 better than 0·8 for all points. A time lag is apparent between the increase in measured and modelled longwave radiation for the sunnier days at the level site (days 74 and 76) and the southeast-facing site (day 70), possibly because direct warming of the canopy by shortwave radiation leads to an immediate increase in longwave radiation emission, but the air is gradually warmed by transfer of sensible heat from the canopy. At the level site, the average radiation is underestimated by 6–8 Wm^{-2} for all radiometers; this could be due to an underestimate of canopy temperatures due to persistent air temperature inversions under the canopy or an overestimate of sky views. Standard deviations of longwave radiation are generally underestimated on the sunnier days at all sites.

Modelled above-canopy longwave radiation is compared with measurements for each site in Figure 2. The model does not capture all the variations in radiation but gives average values quite well; average errors are 7, 16 and −6 Wm^{-2}, and rms errors are 30, 34 and 27 Wm^{-2} for the periods that the array was operated in the southeast facing forest, the level forest and the forest

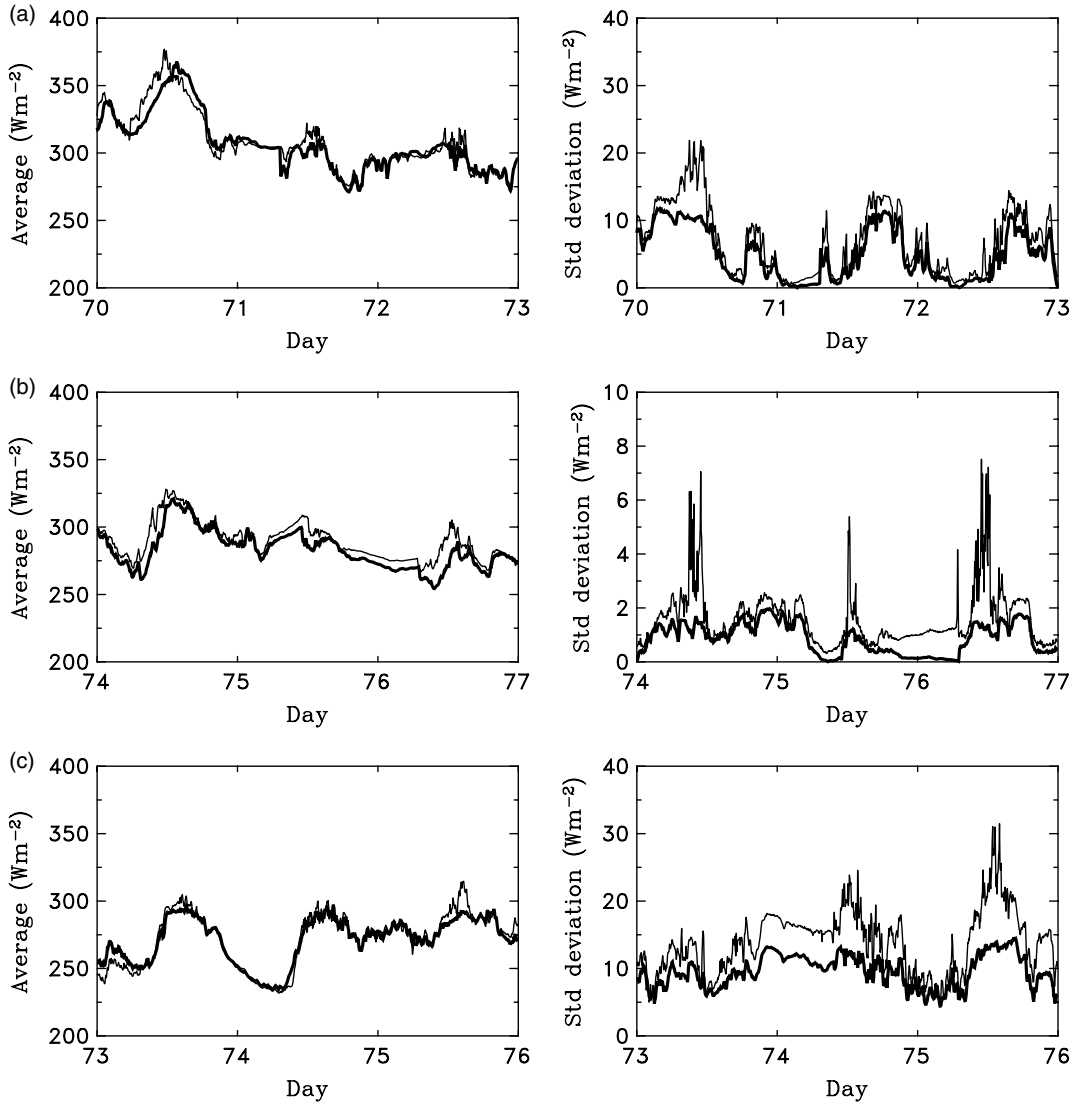

Figure 5. Spatial averages (left) and standard deviations (right) across the radiometer arrays for (a) the southeast-facing forest, (b) the level forest and (c) the forest gap. Thin lines are from measurements and thick lines are from the model using measured sky view, air temperature and above-canopy longwave radiation

DOI: 10.1002/hyp

gap, respectively. Sub-canopy longwave radiation calculated using modelled above-canopy radiation is shown in Figure 6, and statistics for individual radiometers are again given in Tables I–III. A general overestimation of above-canopy radiation reduces the negative bias in sub-canopy radiation at the level site, but rms errors and correlation are generally not as good across the sites as for the model using above-canopy radiation measurements

Bias errors for the multiple linear regression model are zero by construction, so Tables I–III only shows rms errors and correlation for this method; these are better than for the other methods, as can also be seen from the comparisons with measured averages and standard deviations in Figure 7, but the evaluation is not independent of the measurements. The rms errors are close to the estimated uncertainty in the longwave radiation measurements. Regression coefficients are shown in Figure 8 (a)–(c). Weightings increase for longwave radiation and decrease for air temperature with increasing sky view, lying close to $c_{\mathrm{L}} = v$ and $c_{\mathrm{T}} = 1 - v$. The shortwave weighting is small but positive for all radiometers and generally decreases with increasing sky view, suggesting that this term accounts for daytime heating of the canopy above the air temperature, but there is a lot of scatter. A unique relationship would not be expected between shortwave weighting and sky view, as radiative heating of the canopy will depend on how canopy elements are distributed in the hemispherical view; decreasing sky view could both increase the amount of canopy in view and decrease the penetration of shortwave radiation for heating the visible parts of the canopy. Figure 8 (d) shows fractions of temporal variance in sub-canopy longwave radiation explained by each of the input variables. Air temperature explains a greater fraction of variance than above-canopy shortwave radiation, and both show a decrease with increasing sky view, whereas the fraction of variance explained by above-canopy longwave radiation increases and would, of course, exactly match the variance for a completely open site.

The regression model gives better results than the other methods presented above, but this is of limited value as the evaluation data was used in fitting the

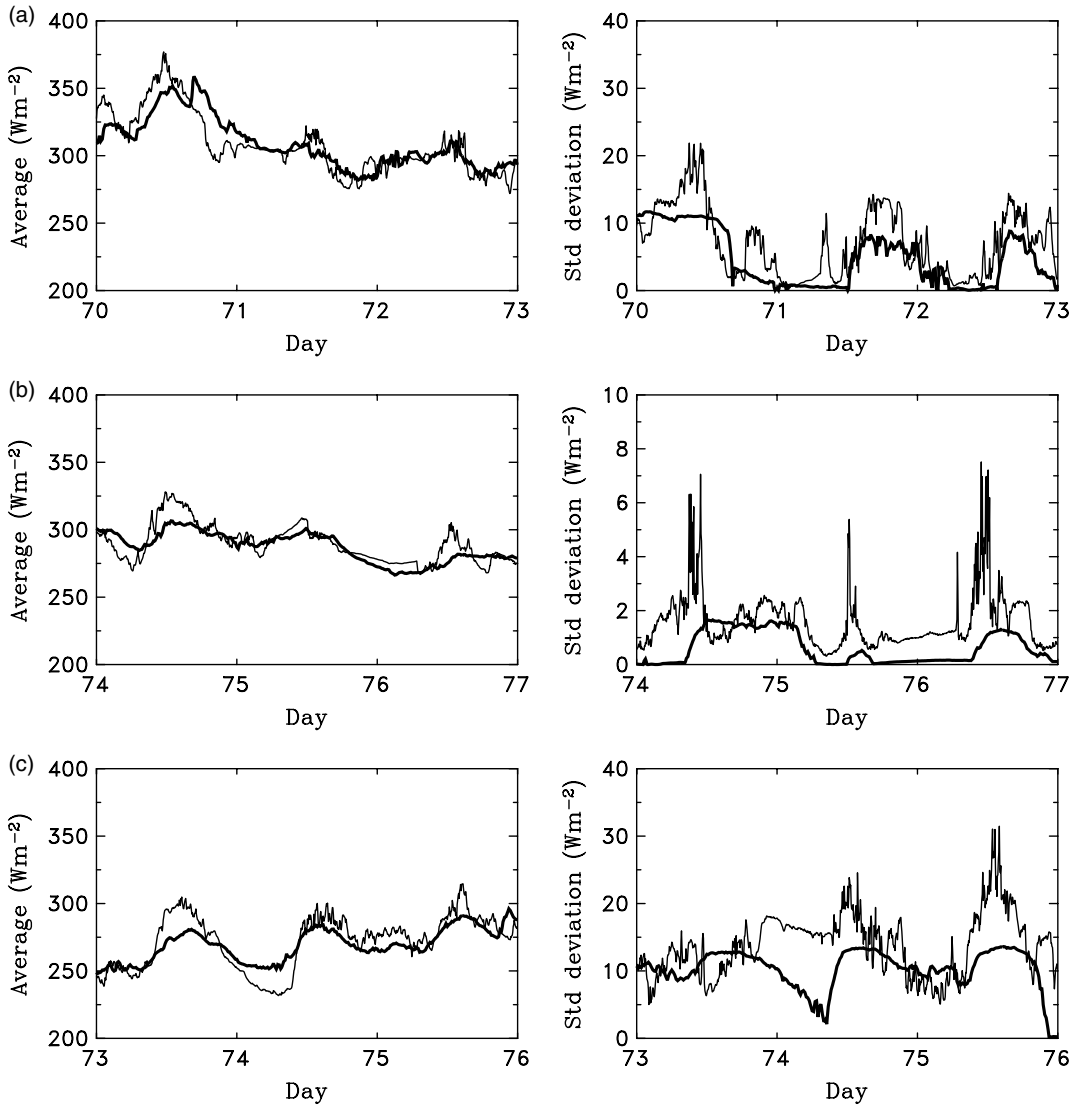

Figure 6. As Figure 5, but for the model using measured sky view and air temperature and modelled above-canopy longwave radiation

DOI: 10.1002/hyp

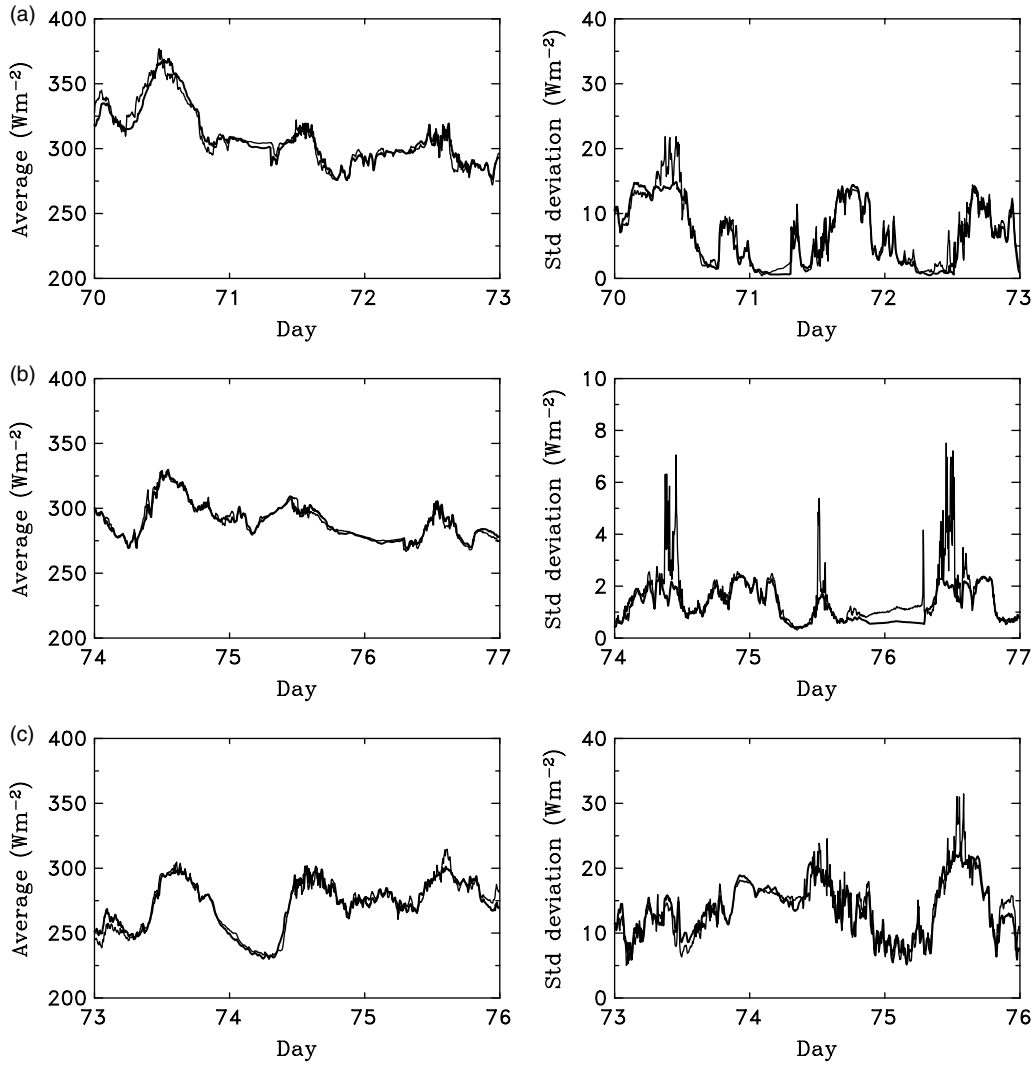

Figure 7. As Figure 5, but for the linear regression model using measured air temperature, above-canopy longwave radiation and above-canopy shortwave radiation

regression coefficients. This method would be of practical use, however, if sub-canopy radiometer data from a short calibration period can be used to predict radiation for other periods with different conditions; a single radiometer, moved between several locations, could then provide coefficients for spatial modelling of sub-canopy radiation. To test this possibility, Equation (9) was fitted to time series from each of the long-term radiometers for the 10-day period 11–20 March 2005. The model was then run on for 120 days up to 19 July 2005 without calibration. Scatter plots of measured and modelled longwave radiation for each radiometer are shown in Figure 9 (a)–(e), and statistics for the calibration and evaluation periods are shown in Table IV. The rms errors in both calibration and evaluation are largest for the most open of the radiometer locations. Although the performance is not as good for the evaluation period as for the calibration period, the rms errors remain better than 10 Wm^{-2} for 15-min averages, and close to or better than 5 Wm^{-2} for daily averages. Figure 9 (f) compares calibration and evaluation rms errors obtained for each radiometer using any 10-day period in the dataset for calibration; it appears that sites and calibration periods giving larger evaluation errors can be identified as they tend to also give larger calibration errors. Results obtained using Equation (1) with measured longwave radiation are almost as good as the regression model results for the evaluation periods, with rms errors ranging from 4·8 to 10·1 Wm^{-2}.

Leaf area index (LAI) is a more commonly used measure of canopy density than sky view and can be measured by remote sensing (Chen and Cihlar, 1996; Riaño *et al.*, 2004), so a relationship between the two would be useful for large-scale modelling of sub-canopy longwave radiation, along with models for variations in air temperature and above-canopy longwave radiation if applied to regions with significant topography (Liston and Elder, 2006). LAI can also be measured by methods based on inversions of Beer's law,

$$\tau = \exp\left[-\frac{G(\theta)}{\sin\theta}\Omega \mathrm{LAI}\right] \qquad (10)$$

where G is a foliage orientation distribution function (Nilson, 1971; Weiss *et al.*, 2004), Ω is a clumping factor

DOI: 10.1002/hyp

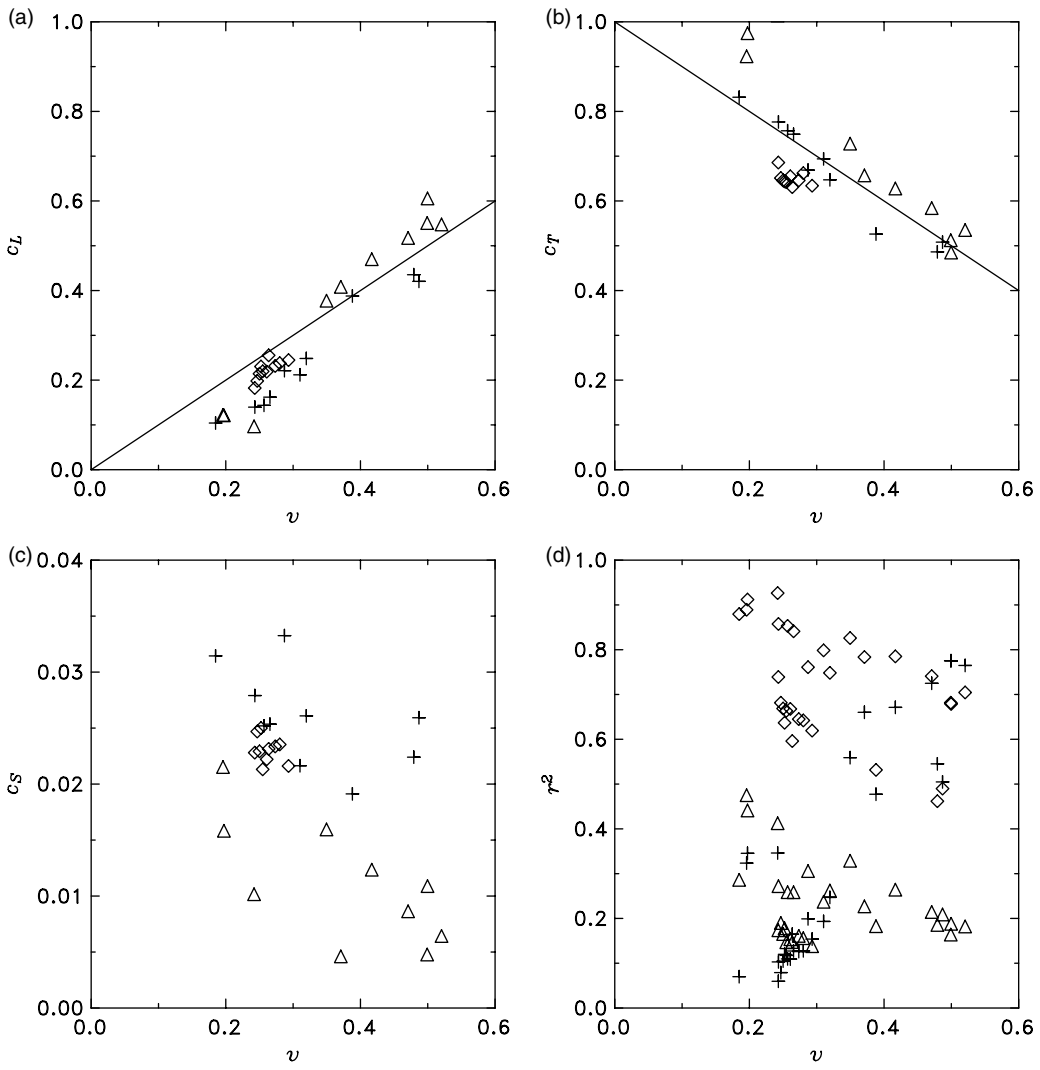

Figure 8. Linear regression coefficients for (a) above-canopy longwave radiation, (b) air temperature and (c) above-canopy shortwave radiation for radiometers at the southeast-facing forest (+), level forest (◊) and forest gap (△) sites. The lines in (a) and (b) are $c_L = v$ and $c_T = 1 - v$. (d) shows the fraction of variance explained by above-canopy longwave radiation (+), air temperature (◊) and above-canopy shortwave radiation (△) for each sub-canopy radiometer

and

$$\tau = \frac{1}{2\pi} \int_0^{2\pi} d\varphi \; c(\theta, \varphi) \tag{11}$$

is calculated from hemispherical photographs or transmission measurements. For the case of horizontal canopy elements, as deduced by Pomeroy and Dion (1996) from shortwave radiation measurements under a pine canopy, $G = \sin\theta$. Substitution in Equation (2) then gives a simple relationship of the form

$$v = \exp(-\Omega \mathrm{LAI}). \tag{12}$$

Based on a literature review, Verseghy *et al.* (1993) used this equation for modelling sub-canopy longwave radiation in the Canadian Land Surface Scheme (CLASS), with $\Omega = 0{\cdot}5$ for needle-leaf trees, and Bartlett *et al.* (2006) tested the sensitivity of CLASS sub-canopy snow simulations to variations in v. Pomeroy *et al.* (2002) obtained a different empirical relationship

$$v = 0{\cdot}45 - 0{\cdot}29 \ln(\mathrm{LAI}) \tag{13}$$

from optical measurements in eight forest stands, but this is close to Equation (12) with $\Omega = 0{\cdot}74$. Leaf area indices and sky views for each of the radiometer locations and the data of Pomeroy *et al.* (2002) are plotted on Figure 10. Most of the points lie close to Equation (12), but those for the radiometers in the forest gap do not; the assumptions behind the relationship between radiation transmission and LAI in Equation (10) do not apply in such locations. Because the gap is small enough that the sky view is restricted by trees around the edge of the gap, optical calculations of LAI give values greater than zero even for points that are not under the canopy.

CONCLUSIONS

Longwave radiation at sites with varying canopy cover has been predicted using three models with different data requirements: an uncalibrated model using measurements of sub-canopy sky view, air temperature and above-canopy longwave radiation; the same model with

DOI: 10.1002/hyp

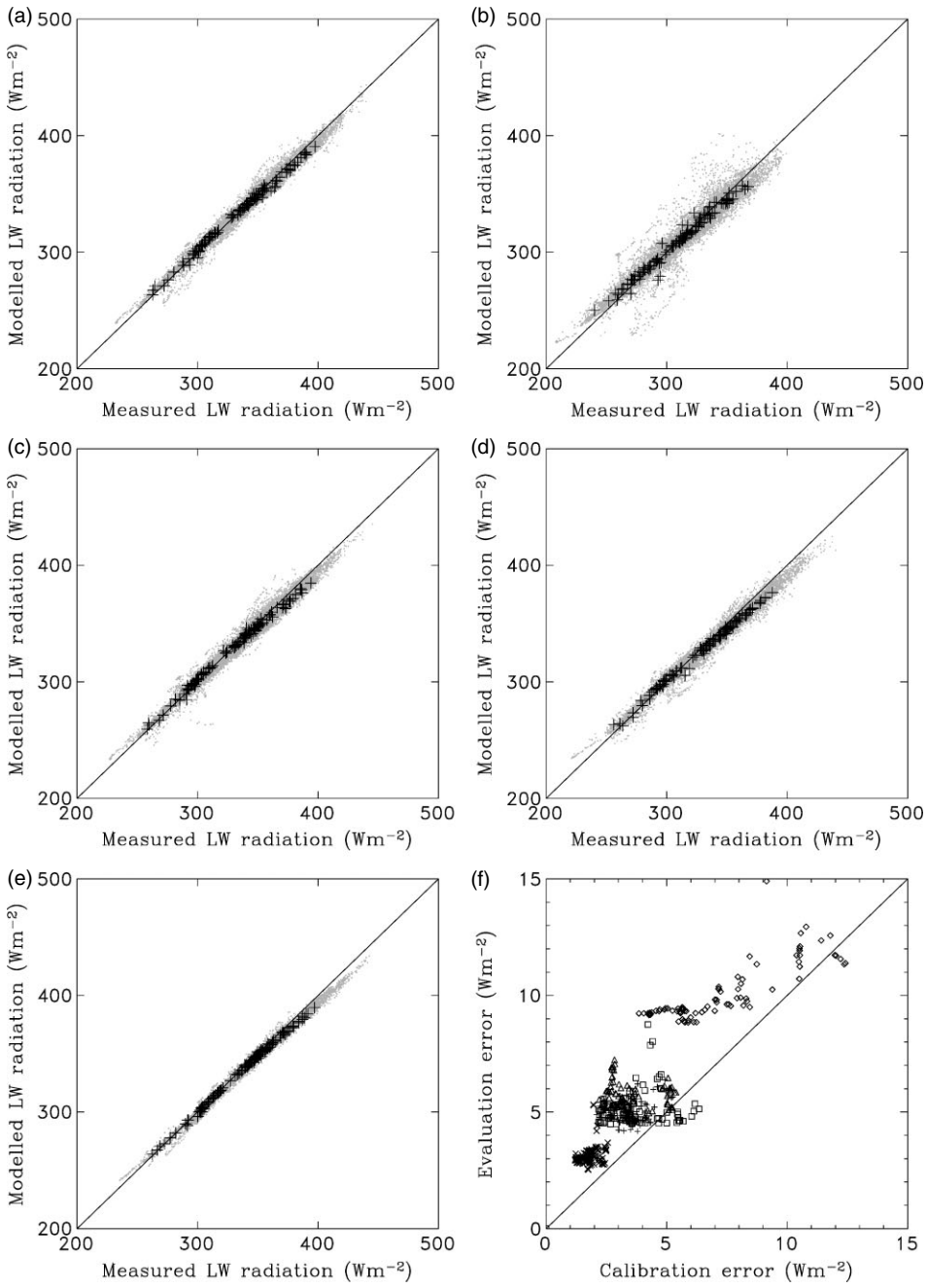

Figure 9. Sub-canopy longwave radiation measured by the five long-term radiometers and modelled by the regression model with a 10-day calibration period. Grey points in (a)–(e) show 15-min averages and black crosses show daily averages. (f) shows evaluation and calibration errors for each possible 10-day calibration period for radiometers 1 (+), 2 (◊), 3 (△), 4 (□) and 5 (×), as listed in Table IV

modelled rather than measured above-canopy longwave radiation; and a model using measured air temperature, above-canopy longwave radiation and above-canopy shortwave radiation calibrated by multiple linear regression against measured sub-canopy longwave radiation. None of the models requires direct measurements of canopy temperatures.

Compared with radiometer array measurements of sub-canopy longwave radiation over 3-day periods at three different sites, the uncalibrated model with measured above-canopy radiation gives rms errors of less than 10 Wm^{-2} in spatial averages for each site and for all but one of the individual radiometer locations. Spatial standard deviations are generally underestimated, and errors for radiometers in a forest gap increase towards the north edge of the gap, where errors due to underestimation of canopy heating by shortwave radiation are expected to be greatest. The modelled above-canopy longwave radiation has less temporal variability than observed, and rms errors for predicted sub-canopy longwave radiation are larger when it is used in place of measurements, but there is little or no degradation in the simulation of sub-canopy longwave radiation averaged over the 3-day periods. The regression model gives the lowest rms errors and highest correlation with measured sub-canopy longwave radiation because its coefficients

DOI: 10.1002/hyp

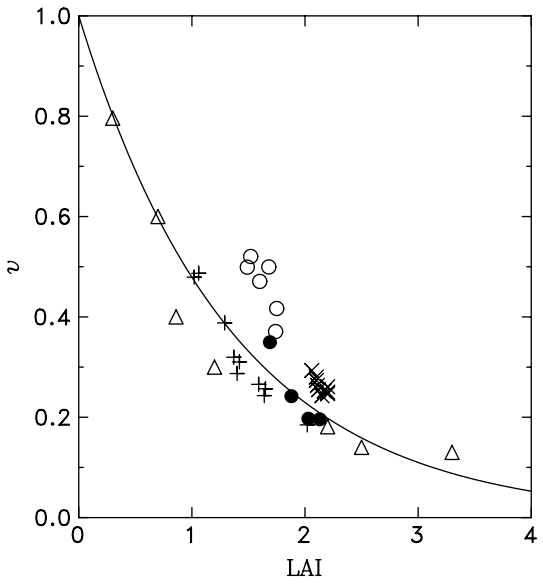

Figure 10. Leaf area index and sky view for each of the radiometers at the southeast-facing forest site (+) and the level forest site (×). Filled circles show results for radiometers that were under the canopy at the forest gap site and open circles are for radiometers in the gap. Triangles show data from Pomeroy *et al*. (2002) and the line is given by Equation (11) with $\Omega = 0{\cdot}74$

are fitted by minimization of rms errors. Weightings for above-canopy shortwave radiation are positive for all radiometer locations, suggesting that the model calibration is compensating for underestimates in canopy temperature due to solar heating. Although the regression model requires sub-canopy radiation measurements for calibration, it was found that the model could be run for longer periods with little degradation in results after a 10-day calibration period. Sites and calibration periods for which the calibration errors are larger generally appear to give larger evaluation errors, so the accuracy of the model can be estimated *a priori*.

Hemispherical photographs provide a useful means of estimating sky view at field sites, but estimates of sky view can also be made using leaf area index, which can be mapped over larger areas using standard remote sensing techniques. It should be noted that the techniques shown here are strictly empirical, but such techniques may prove useful in helping to define scaling functions for more physically based techniques of estimating sub-canopy longwave and are instructive as to the primary driving factors.

ACKNOWLEDGEMENTS

The authors would like to thank Michael Solohub for assistance in the field and maintenance of the Marmot Creek Research Basin. Danny Marks and Janet Hardy are thanked for the loan of radiometers and discussion of the experiment. The MicroMet code was supplied by Glen Liston. Financial support was provided by the Natural Environment Research Council (UK), the Natural Sciences and Engineering Research Council of Canada, the NOAA GEWEX Americas Prediction Project (USA), the Canada Research Chairs Programme and the Canadian Foundation for Climate and Atmospheric Sciences. Logistical support was kindly provided by the University of Calgary Kananaskis Field Station, directed by Professor Ed Johnson.

REFERENCES

Anderson MC. 1964. Studies of the woodland light climate I. The photographic computation of light condition. *Journal of Ecology* **52**: 27–41.

Bartlett PA, MacKay MD, Verseghy DL. 2006. Modified snow algorithms in the Canadian Land Surface Scheme: model runs and sensitivity analysis at three boreal forest stands. *Atmosphere-Ocean* **44**: 207–222.

Bowling LC, Lettenmaier DP, Nijssen B, Graham LP, Clark DB, Maayar MEl, Essery RLH, Goers S, Gusev YM, Habets F, van den Hurk B, Kahan Jin J, Lohmann D, Ma X, Mahanama S, Mocko D, Nasonova O, Niu G-Y, Samuelsson P, Shmakin AB, Takata K, Verseghy D, Viterbo P, Xia Y, Xue Y, Yang Z-L. 2003. Simulation of high latitude hydrological processes in the Torne-Kalix basin: PILPS Phase 2e. 1: experiment design and summary intercomparisons. *Global and Planetary Change* **38**: 1–30.

Chen JM, Cihlar J. 1996. Retrieving leaf area index of boreal conifer forests using Landsat TM images. *Remote Sensing of Environment* **55**: 153–162.

Danby RK, Hik DS. 2007. Variability, contingency and rapid change in recent subarctic alpine tree line dynamics. *Journal of Ecology* **95**: 352–363.

Essery R, Bunting P, Hardy J, Link T, Marks D, Melloh R, Pomeroy J, Rowlands A, Rutter N. 2007. Radiative transfer modelling of a coniferous canopy characterized by airborne remote sensing. *Journal of Hydrometeorology* (in press).

Evans GD, Coombe DE. 1959. Hemispherical and woodland canopy photography and the light climate. *Journal of Ecology* **47**: 103–113.

Fairall CW, Persson POG, Bradley EF, Payne RE, Anderson SP. 1998. A new look at calibration and use of Eppley Precision Infrared Radiometers. Part I: theory and application. *Journal of Atmospheric and Oceanic Technology* **15**: 1229–1242.

Faria D, Pomeroy JW, Essery RLH. 2000. Effect of covariance between ablation and snow water equivalent on depletion of snow-covered area in a forest. *Hydrological Processes* **14**: 2683–2695.

Frazer GW, Canham CD, Lertzman KP. 1999. *Gap Light Analyzer (GLA): Users Manual and Program Documentation, Version 2·0*. Simon Fraser University: Burnaby, British Columbia.

Gray DM. 1970. *Handbook on the Principles of Hydrology*. Canadian National Committee for the International Hydrological Decade: Ottawa.

Iziomon MG, Mayer H, Matzarakis A. 2003. Downward atmospheric longwave irradiance under clear and cloudy skies: measurement and parameterization. *Journal of Atmospheric and Solar-Terrestrial Physics* **65**: 1107–1116.

Link TE, Hardy JP, Marks D. 2004. A deterministic method to characterize canopy radiative transfer properties. *Hydrological Processes* **18**: 3583–3594.

Liston GE, Elder K. 2006. A meteorological distribution system for high-resolution terrestrial modelling (MicroMet). *Journal of Hydrometeorology* **7**: 217–234.

López-Moreno JI, Latron J. 2008. Influence of canopy density on snow distribution in a temperate mountain range. *Hydrological Processes* **22**: 117–126. DOI: 10.1002/hyp.6572.

Lundberg A, Nakai Y, Thunehed H, Halldin S. 2004. Snow accumulation in forests from ground and remote-sensing data. *Hydrological Processes* **18**: 1941–1955.

Metcalfe RA, Buttle JM. 1998. Statistical model of spatially distributed snowmelt rates in a boreal forest basin. *Hydrological Processes* **12**: 1701–1722.

Nilson T. 1971. A theoretical analysis of the frequency of gaps in plant stands. *Agricultural Meteorology* **8**: 25–38.

Pomeroy JW, Dion K. 1996. Winter radiation extinction and reflection in a boreal pine canopy: measurements and modelling. *Hydrological Processes* **10**: 1591–1608.

Pomeroy JW, Gray DM, Hedstrom NR, Janowicz JR. 2002. Prediction of seasonal snow accumulation in cold climate forests. *Hydrological Processes* **16**: 3543–3558.

Pomeroy JW, Marks D, Ellis C, Essery RLH, Link T, Hardy J, Rowlands A. 2007. The influence of canopy temperature on incoming longwave radiation to snow in coniferous forests. *Hydrological Processes* (Submitted).

Riaño D, Valladares F, Condés S, Chuvieco E. 2004. Estimation of leaf area index and covered ground from airborne laser scanner (LiDAR) in two contrasting forests. *Agricultural Meteorology* **124**: 269–275.

Rich PM, Wood J, Vieglais DA, Burek K, Webb N. 1999. *Hemiview User Manual*. Delta-T Devices Ltd: Cambridge.

Sellers PJ, Mintz Y, Sud YC, Dalcher A. 1986. A Simple Biosphere Model (SiB) for use within General circulation Models. *Journal of the Atmospheric Sciences* **43**: 505–531.

Sicart J-E, Pomeroy JW, Essery RLH, Hardy J, Link T, Marks D. 2004. A sensitivity study of daytime net radiation during snowmelt to forest canopy and atmospheric conditions. *Journal of Hydrometeorology* **5**: 774–784.

Slater AG, Schlosser CA, Desborough CE, Pitman AJ, Henderson-Sellers A, Robock A, Vinnikov KYa, Mitchell K, Boone A, Braden H, Chen F, Cox PM, Rosnay Pde, Dickinson RE, Dai Y-J, Duan Q, Entin J, Etchevers P, Gedney N, Gusev YeM, Habets F, Kim J, Koren V, Kowalczyk EA, Nasonova ON, Noilhan J, Schaake S, Shmakin AB, Smirnova TG, Verseghy D, Wetzel P, Xue Y, Yang Z-L, Zeng Q. 2001. The representation of snow in land surface schemes: results from PILPS 2(d). *Journal of Hydrometeorology* **2**: 7–25.

Verseghy DL, McFarlane NA, Lazare M. 1993. CLASS—A Canadian land surface scheme for GCMs, II. Vegetation model and coupled runs. *International Journal of Climatology* **13**: 347–370.

Weiss M, Baret F, Smith GJ, Jonckheere I, Coppin P. 2004. Review of methods for in situ leaf area index (LAI) determination. Part II: estimation of LAI, errors and sampling. *Agricultural Meteorology* **121**: 37–53.

Yang Z-L, Dickinson RE, Robock A, Vinnikov KY. 1997. On validation of the snow sub-model of the Biosphere-Atmosphere Transfer Scheme with Russian snow cover and meteorological observational data. *Journal of Climate* **10**: 353–373.

DOI: 10.1002/hyp